Journal of Solid State Chemistry 182 (2009) 107–114

Contents lists available at ScienceDirect

Journal of Solid State Chemistry

journal homepage: www.elsevier.com/locate/jssc

Local structure of Cu in $Cs_8Na_{16}Cu_5Ge_{131}$ type II clathrate

A.N. Mansour [a,*], M. Beekman [b], W. Wong-Ng [c], G.S. Nolas [b]

[a] Systems and Materials for Power and Protection Branch, Naval Surface Warfare Center, Carderock Division, West Bethesda, MD 20817-5700, USA
[b] Department of Physics, University of South Florida, Tampa, FL 33620, USA
[c] Materials Science and Engineering Laboratory, National Institute of Standards and Technology, Gaithersburg, MD 20899, USA

ARTICLE INFO

Article history:
Received 2 July 2008
Received in revised form
10 September 2008
Accepted 20 September 2008
Available online 17 October 2008

Keywords:
Thermoelectrics
Clathrates
X-ray absorption spectroscopy
Atomic structure

ABSTRACT

We have used X-ray absorption spectroscopy (XAS) to investigate the local structure of Cu and Ge in the $Cs_8Na_{16}Cu_5Ge_{131}$ type II clathrate. We show that the local structure parameters for Ge (coordination number and distances) are consistent with those derived on the basis of XRD investigation of $Cs_8Na_{16}Ge_{136}$. The EXAFS data suggest that Cu either randomly substitutes for Ge on the clathrate framework or preferentially on the 96*g* site but not preferentially on the 32*e* or 8*a* sites (Wyckoff notation). Furthermore, we find that the Cu–Ge distance is smaller than the Ge–Ge distance by 0.13 Å, indicating a local distortion around the Cu atoms. The estimated degrees of disorder for Cu–Ge and Ge–Ge interactions indicate the Cu–Ge clathrate framework to be relatively stiff, while those for Na–Ge and Cs–Ge interactions corroborate previous observations of strong thermal disorder of the alkali guests in these materials. Our XAS results offer insight into the site substitution of Cu in this material, information unattainable from X-ray diffraction due to the lack of scattering contrast between Cu and Ge.

Published by Elsevier Inc.

1. Introduction

Group 14 derived intermetallic clathrate phases exhibit cage-like structural features with direct relationships to the intriguing physical properties they possess. In these materials, a covalently bonded host framework composed of group 14 elements (e.g. Si, Ge, or Sn) or substituents can house guest atomic species inside intrinsic polyhedral voids. The interaction between guest and host framework in these crystalline materials results in a range of scientifically and technologically important characteristics, including exceptional thermoelectric properties [1], glass-like thermal conductivity [2], magnetic phenomena [3,4] and superconductivity [5].

The crystal structures of intermetallic clathrates can be classified into several primary structure types, of which those exhibiting the type I clathrate crystal structure have been most extensively studied [6,7]. Recently, materials possessing the type II clathrate crystal structure have received rapidly increasing interest [8]. This class of materials offers a structure type within which rich possibilities exist for investigation of new compositions of intermetallic clathrates.

In order to explore the compositional possibilities as well as effects on physical properties, investigation of framework substitution in type II intermetallic clathrates has recently been initiated both experimentally [9–11] and theoretically [12]. Recently [11] by substitution of Cu for Ge in $Cs_8Na_{16}Cu_5Ge_{131}$, it was shown that the electrical and thermal transport properties are indeed influenced by framework substitution. In the case of $Cs_8Na_{16}Cu_5Ge_{131}$, determination of any site preference for Cu using conventional X-ray diffraction (XRD) techniques is difficult due to the very small X-ray scattering contrast between Cu and Ge. Extended X-ray absorption fine structure (EXAFS) analysis is an ideal tool to gain detailed information on the local structural features for the absorbing atom. Herein, we provide insight into the local structural environment and site occupation of Cu in $Cs_8Na_{16}Cu_5Ge_{131}$, studied by EXAFS.

2. Experimental

2.1. Preparation and characterization

The $Cs_8Na_{16}Cu_5Ge_{131}$ specimen reported on here is the same as that reported on in Ref. [11], the preparation procedure for which has been described previously [9,11]. High purity Ge (intrinsic) and Cu (99.9%) powders were thoroughly pre-mixed in the Cu:Ge molar ratio of 5:131, and then Cs (99.98%) and Na (99.95%) metal added to the mixture in a nitrogen filled glove box. The mixture

* Corresponding author. Fax: +301 227 5480.
E-mail addresses: azzam.mansour@navy.mil (A.N. Mansour), gnolas@cas.usf.edu (G.S. Nolas).

0022-4596/$ - see front matter Published by Elsevier Inc.
doi:10.1016/j.jssc.2008.09.024

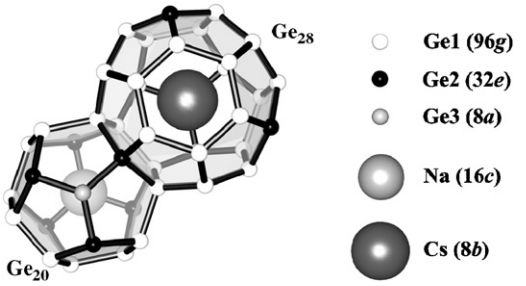

Fig. 1. The Ge_{20} and Ge_{28} polyhedra that form the framework of the $Cs_8Na_{16}Ge_{136}$ type II clathrate.

was reacted inside a tungsten crucible sealed under nitrogen inside a stainless steel reaction vessel. The mixtures were heated at 800 °C for two days, then held at 650 °C for one week, and then slowly cooled to room temperature.

Powder XRD and Rietveld structural refinements [11] indicated the specimen to be well crystallized with the type II clathrate crystal structure. This structure may be conceptualized by considering the polyhedra shown in Fig. 1. Space filling pentagonal dodecahedra (E_{20}) and hexacaidecahedra (E_{28}) share faces in the ratio 2:1 to form the face-centered cubic type II clathrate crystal structure (space group $Fd\bar{3}m$). The three non-equivalent crystallographic sites 96*g*, 32*e*, and 8*a* (Wyckoff notation) comprise the framework, while guest atoms are situated at the 8*b* (E_{28} cage) and 16*c* (E_{20} cage) sites.

Energy dispersive spectroscopy (EDS) confirmed the Cu:Ge ratio within the clathrate to be 5:131 within experimental uncertainty. This composition was further confirmed by XAS measurements as discussed below. A trace amount of elemental Ge (~1 wt% as estimated from Rietveld refinement) was detected in the specimen; no other impurity phases were detected from XRD or EDS.

2.2. X-ray absorption spectroscopy experiments

The XAS experiments were conducted on the bending magnet station X-11A of the National Synchrotron Light Source with the electron storage ring operating at electron energy of 2.58 GeV and a stored current in the range of 200–300 mA [13]. The Cu *K*-edge (8979 eV) and Ge *K*-edge (11103 eV) X-ray absorption fine structure (XAFS) spectra were collected in the transmission mode using two flat Si(111) double crystal monochromator. The harmonic-content of the beam was minimized by adjusting the parallelism of the monochromator crystals to reduce the peak intensity by 40% for the Cu data and by 20% for the Ge data. The incident and transmitted beam intensities were monitored using ionization chambers (30 cm in length) while continuously flowing appropriate combination of nitrogen and argon through the chambers. The incident beam chamber had 100% nitrogen (Cu data) and 90% nitrogen+10% argon (Ge data) while the transmitted beam chamber had 85% nitrogen and 15% Ar (Cu data) and 60% nitrogen+40% Ar (Ge data). A third ionization chamber (15 cm in length) with the same gases as the second chamber was used to collect the transmitted beam intensity for the reference foil. The $Cs_8Na_{16}Cu_5Ge_{131}$ specimen was mounted in a standard liquid nitrogen dewar and the spectra were collected at room temperature (RT, 298 K) and near the liquid nitrogen temperature (LNT, 77 K). The energy calibration of the monochromator was monitored using a 7.5 μm thick Cu foil and a 325 mesh Ge powder.

The $Cs_8Na_{16}Cu_5Ge_{131}$ material was ground and sifted through a 325 mesh. Approximately 18 mg of the sifted powder was thoroughly mixed with 100 mg of boron nitride and then 102 mg of the mixture was retrieved and pressed into a self supporting rectangular pellet with dimensions of 5 mm × 12 mm. The Cu and Ge X-ray absorption *K*-edge jumps for $Cs_8Na_{16}Cu_5Ge_{131}$ were determined to be 0.092 and 3.18, respectively. The 325 mesh Ge powder specimen had a X-ray absorption *K*-edge jump of 2.30.

From the standpoint of minimizing the statistical errors in an absorption experiment, it is desirable to adjust the sample thickness so that the total absorption above the edge is near 2.6 [14]. However, other considerations, such as the thickness effect or pinholes make it highly desirable to have the absorption edge jump smaller than 1.5 [15]. Furthermore, for powder material which is the case here, the size effect makes it also desirable to have particles as fine as possible, preferably, smaller than the 400 mesh particles [16]. It is to be noted that both the thickness and size effects can lead to reduction in the amplitude of the EXAFS signal but do not affect the phases of the EXAFS signal and hence, the measured distances are not altered in any way.

In our case, the absorption above the Ge *K*-edge is near 4. The implications of this are (i) reduction in the amplitude of the EXAFS signal due to pinholes and size effect (ii) some decrease in the signal to noise ratio of our spectra. However, based on the values of the amplitude reduction factor listed in Table 2, our sample appears to have relatively uniform thickness and amplitude reductions due to sample inhomogeneity should not be a significant issue. With the high intensity of X-rays provided by synchrotron sources the signal to noise ratio of our spectra is also not an issue at all as can be confirmed by the extremely high quality of our spectra recorded later in the paper. As described later in the text, a number of spectra were averaged in our case to further enhance the signal to noise ratio of our spectra.

Despite the small Cu *K*-edge jump of 0.09, we have elected to collect the Cu XAFS spectra in the transmission rather than the fluorescence mode for the following reasons. Measurements in the fluorescence mode are appropriate only when one of two conditions is satisfied [17]. One condition is the thin film limit and is appropriate for highly concentrated samples. The other condition is the infinitely thick film limit and is appropriate for extremely dilute samples. In our case, none of these conditions can be truly satisfied. In addition, for the Cu *K*-edge, the fluorescence mode is not the dominant decay process. The fluorescence mode competes with the Auger mode and the fluorescence yield is only 0.44 [18]. Hence, the signal to noise ratio in the fluorescence mode will be reduced by the relatively low fluorescence yield. Furthermore, interference with the fluorescence signal from Cs will undoubtedly compromise the quality of the Cu fluorescence signal to some degree. This is significant considering that the total yield for the Cs L-edges is 0.23 and that the ratio of Cs/Cu is 1.6. Finally, the amplitudes of fluorescence spectra are altered by the well-known self absorption by the sample [19,20] and the energy dependence of the incident beam absorption and must be corrected for these effects. These corrections involve approximations that could introduce unnecessary errors to the spectra. Therefore, measurement of the X-ray absorption spectra in the fluorescence mode usually is used as a last resort when it cannot be made in the transmission mode. With the high quality of Cu *K*-edge EXAFS spectra presented in our paper, extending to about 16 $Å^{-1}$ for the liquid nitrogen data, there is no significant advantage to collect the Cu spectra in the fluorescence mode.

2.3. X-ray absorption spectroscopy data analysis

The Cu *K*-edge and Ge *K*-edge spectra of $Cs_8Na_{16}Cu_5Ge_{131}$ were calibrated by setting the inflection point energy for elemental Cu and Ge to 8979.0 and 11103, respectively. A number of spectra

were collected at each temperature and were averaged to enhance the signal to noise ratio of the absorption spectra. The monochromator was extremely stable during multiple scans and no energy shifts were observed from one scan to the next over a range of 20 scans. The RT and the near LNT Cu *K*-edge data consist of the average of 14 and 17 spectra, respectively. The RT as well as the near LNT Ge *K*-edge data consists of the average of five spectra [21]. The RT Ge *K*-edge data for elemental Ge consists of the average of 3 spectra. The *K*-edge absorption was isolated by fitting the pre-edge region (−300 to −100 eV relative to the edge energy) with the Victoreen formula, extrapolating over the entire range of the spectrum, and subtracting the pre-edge background from the entire spectrum. Energy independent step normalization was applied by dividing the absorption cross section with the value of the average absorption in the energy range 200–500 eV above the edge energy. The photoelectron wave number was derived by setting the inner potential to 8979.0 eV (Cu data) and 11 103 eV (Ge data). The EXAFS data, $\chi(k)$, were extracted using multi-node cubic spline procedures over the *k*-range of 2.0–16.7 $Å^{-1}$ (Cu data) and 2.0–19.0 $Å^{-1}$ (Ge data). The post-edge background was optimized by minimizing the amplitude of non-physical peaks in the 0–1.2 Å region of the Fourier transform [22,23]. The data analysis up to this point was carried out using the WinXAS software package (version 3.1) [24,25].

All fits were made using the curve fitting code FEFFIT (version 2.984) of the University of Washington XAFS (UWXAFS) software package [26]. The data were fitted using theoretical standards calculated based on the curved-wave scattering formalism of the FEFF code (version 8.2) [27,28]. The FEFF calculations were performed using established structural models for elemental Ge [29] and the $Cs_8Na_{16}Ge_{136}$ [9] standards. The local structure parameters for the first few coordination spheres around Ge in $Cs_8Na_{16}Ge_{136}$ are listed in Table 1. Note that the three non-equivalent sites are labeled as Ge1 (96*g*), Ge2 (32*e*), and Ge3 (8*a*); the nearest neighbor coordination environments and site symmetries for the three sites are shown in Fig. 2. Due to the high degree of symmetry of the Ge3 site (see Fig. 2), it was used in the FEFF code to calculate the backscattering amplitudes and phase shifts for Ge–Ge interactions. The phase shift for the central Cu atom was calculated using the same cluster data for the Ge3 site while placing a Cu atom at the origin of the cluster. In Table 1, we also included the local structure parameters for the first two coordination spheres of elemental Ge for comparison purposes.

The Fourier transforms were generated using k^1-weighted EXAFS spectra over the k_{min}–k_{max} range of 3.0–16.0 $Å^{-1}$ with a Hanning window of 1.0 $Å^{-1}$. The fits were performed in real space over the R_{min}–R_{max} ranges of 1.56–2.42 Å (Cu data) and 1.50–2.79 Å (Ge data). The RT and LNT data for each of the Cu *K*-edge and the Ge *K*-edge spectra of $Cs_8Na_{16}Cu_5Ge_{131}$ were simultaneously fitted in order to reduce the correlation between the many body amplitude reduction factor and the disorder of the system. In fitting the data, the many body amplitude reduction

Table 1
Summary of local structure parameters derived on the basis of available single crystal X-ray diffraction results for $Cs_8Na_{16}Ge_{136}$ [9], and elemental Ge [22] in the diamond structure

$Cs_8Na_{16}Ge_{136}$						Elemental Ge	
1st shell							
X–*Y* pair[a]	*N* at *R* (Å)	*X*–*Y* pair	*N* at *R* (Å)	*X*–*Y* pair	*N* at *R* (Å)	*X*–*Y* pair	*N* at *R* (Å)
Ge1–Ge2 (d_1)	1 at 2.490	Ge2–Ge3 (d_4)	1 at 2.485	Ge3–Ge2 (d_4)	4 at 2.485	Ge–Ge	4 at 2.450
Ge1–Ge1 (d_2)	2 at 2.501	Ge2–Ge1 (d_1)	3 at 2.490				
Ge1–Ge1 (d_3)	1 at 2.505						
Average Ge–Ge	4 at 2.499		4 at 2.489		4 at 2.485		
2nd shell							
Ge1–Na	2 at 3.542	Ge2–Na	3 at 3.445	Ge3–Na	4 at 3.354		
Ge1–Ge2	2 at 3.966	Ge2–Ge1	6 at 3.966				
Ge1–Ge3	1 at 4.002			Ge3–Ge1	12 at 4.002	Ge–Ge	12 at 4.001
Ge1–Ge2	1 at 4.046	Ge2–Ge1	3 at 4.046				
Ge1–Ge1	4 at 4.072	Ge2–Ge2	3 at 4.058				
Ge1–Ge1	2 at 4.123						
Ge1–Cs	1 at 4.140						
Ge1–Cs	1 at 4.226	Ge2–Cs	1 at 4.223				
Ge1–Ge1	2 at 4.327						
Average Ge–Ge	12 at 4.097		12 at 4.009		12 at 4.002		

The distance *R* between each atom *X* and *Y* is given, along with the distance multiplicity *N*; see Fig. 2 for reference.
[a] According to the Wyckoff notation, the Ge1, Ge2, and Ge3 correspond to the 96*g*, 32*e*, and 8*a* sites, respectively.

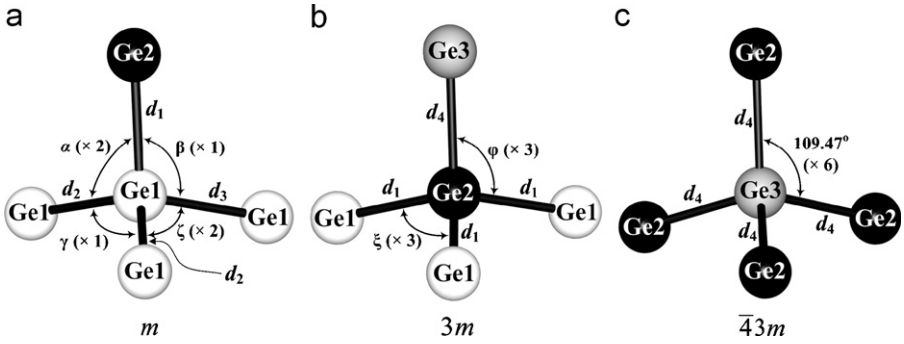

Fig. 2. Nearest neighbor coordination environments for the (a) Ge1 (96*g*), (b) Ge2 (32*e*), and (c) Ge3 (8*a*) framework sites. The d_n distances of Table 1 are indicated, as well as indication of the distinct bond angles and site symmetries.

factor (S_0^2), coordination distance (R), mean square relative disorder (σ^2), and inner potential correction (E_0) were used as floating parameters. The coordination numbers were constrained to the well-established crystallographic values listed in Table 1. A Gaussian disorder was assumed for all shells. Amplitude correction for McMaster normalization was made using values determined by the software code Atoms. The number of fitting parameters was kept below the maximum number of independent data points allowed by the Brillouin theorem [30]. The goodness of each model was monitored by the value of the R-factor, which is the sum of the square of residuals between measured and model data normalized to the magnitude of the measured data. Quantitative curve fit analysis was limited to the first shell of atoms. It is not possible to uniquely fit the second shell of atoms because of the large number of single scattering paths contributing in this region. Simulations using XRD results for the first and second shells will be discussed later in the text.

3. Results

A comparison of the raw and normalized Cu and Ge K-edge XAFS spectra collected near the LNT for $Cs_8Na_{16}Cu_5Ge_{131}$ are displayed in Fig. 3. As can be seen from the raw data, the Ge K-edge jump is significantly larger than the Cu K-edge jump due to the higher Ge concentration relative to the Cu concentration in the specimen. The absorption edge jumps are 0.092 and 3.18 for Cu and Ge, respectively. Taking into account the theoretical edge jumps for Cu and Ge of 26 485 and 20 068 Barns/atom [31], respectively, the atomic ratio of Ge to Cu in the specimen is determined to be 26.19. This value compares very well with the nominal value of 26.20, which is calculated on the basis of the stoichiometry of the specimen. Once the spectra are normalized per Cu or Ge atom, the EXAFS oscillations (or wiggles) are clearly prominent in the XAFS spectra for both Cu and Ge. These oscillations extend several hundred eV above the edge energy for both Cu and Ge.

A comparison of the RT and the near LNT of Ge K-edge EXAFS spectra and the corresponding k-weighted Fourier transforms are shown in Fig. 4. It is to be noted that the EXAFS spectra and Fourier transforms of Ge represent an ensemble average of the local structure of three non-equivalent sites of Ge, namely, Ge1, Ge2 and Ge3. Furthermore, the distances of various coordination spheres in the Fourier transforms are shifted lower by about 0.2–0.3 Å relative to real distances due to the phase shifts of the central and backscattering atoms. The apparent contractions in the Fourier transforms distances are accounted for during the quantitative analysis of the EXAFS spectra. As anticipated, the amplitude of the EXAFS oscillations as well as the amplitude of

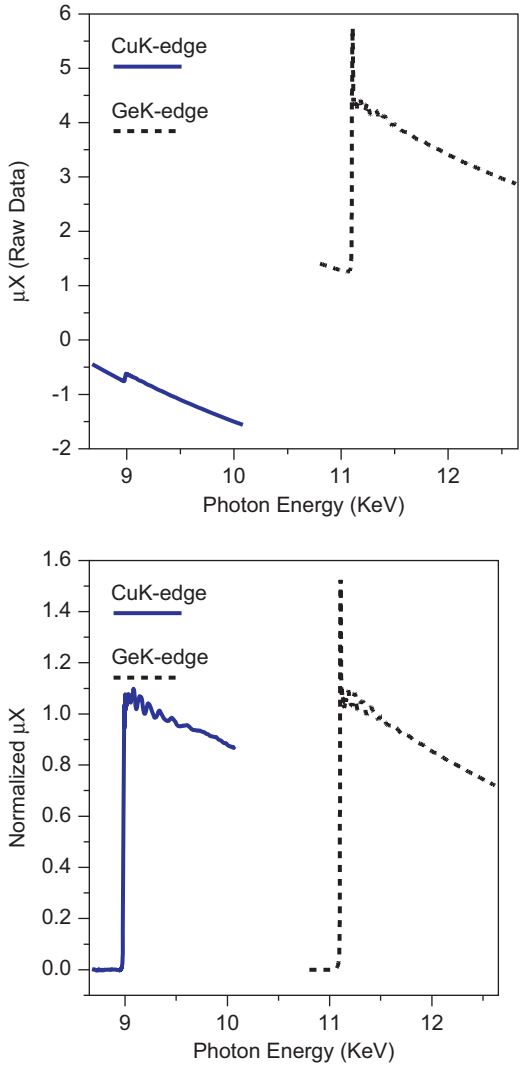

Fig. 3. Raw (top) and normalized (bottom) Cu and Ge K-edge XAFS spectra for $Cs_8Na_{16}Cu_5Ge_{131}$ collected at near the temperature of liquid nitrogen (LN).

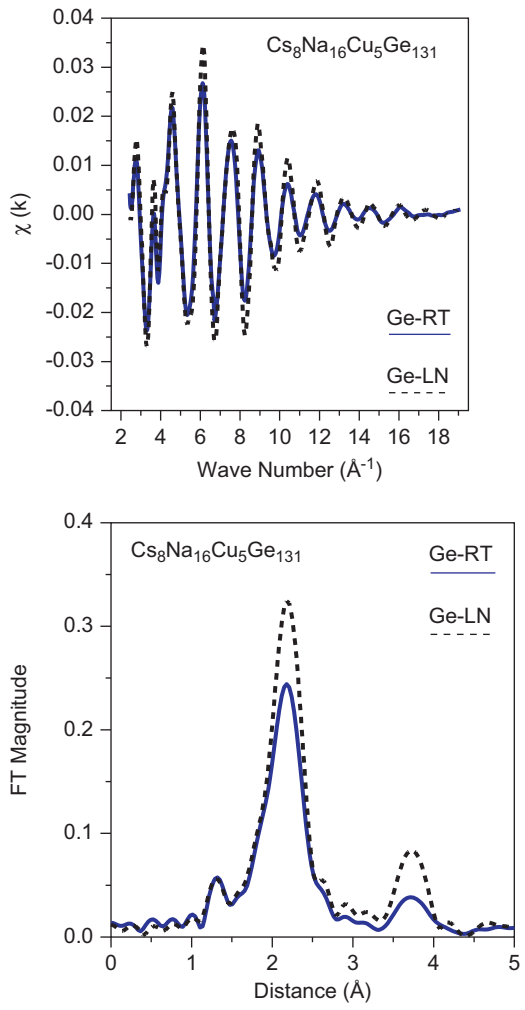

Fig. 4. Comparison of Ge K-edge EXAFS (top) and Fourier transforms (bottom) for $Cs_8Na_{16}Cu_5Ge_{131}$ collected at room temperature (RT) and near the temperature of liquid nitrogen (LN).

Table 2
Summary of local structure parameters as determined from analysis of XAFS spectra

Specimen	T	X–Y pair	S_0^2	R (Å)	σ^2 (10^{-3} Å^2)	R-factor
$Cs_8Na_{16}Cu_5Ge_{131}$	RT	Cu–Ge	0.74±0.03	2.354±0.004	4.34±0.46	0.005
	LN	Cu–Ge	0.74±0.03	2.349±0.003	2.32±0.29	0.006
	RT	Ge–Ge/Cu	0.80±0.05	2.486±0.007	4.73±0.61	0.020
	LN	Ge–Ge/Cu	0.80±0.05	2.481±0.005	2.82±0.42	0.015
Ge powder	RT	Ge–Ge	0.70±0.04	2.444±0.003	3.46±0.37	0.004

S_0^2 is the many body amplitude reduction factor which accounts for inelastic losses within the central absorbing atom. R is the coordination distances. σ^2 mean squares relative displacement for the X–Y pair of atoms, which includes both thermal and static disorder. R-factor is a measure of the goodness of fit for the model used to fit the experimental data.

the Fourier transforms increased when the specimen temperature decreased from RT to the LNT due to the quenching of the thermal motion of the atoms. The Fourier transforms display a major peak centered around 2.2 Å, which corresponds to the first coordination sphere of the tetrahedral coordination of framework Ge atoms. The peak centered near 3.7 Å corresponds to the more distant Ge–Ge coordination spheres (see Table 2). Due to the rattling behavior of the Cs and Na atoms [32,33], these atoms possess high degrees of thermal disorder and, therefore, the contributions of the Ge–Na and Ge–Cs interactions are very small and can be ignored. As we show later in the text, the total disorder for each of the Ge–Na and Ge–Cs interactions was estimated to be greater than 0.02 Å^2. The high degree of disorders for Ge–Na and Ge–Cs were necessary in order for the simulated Fourier transforms derived on the basis of local structure parameters from XRD data (Table 1) to closely resemble the Fourier transforms of the experimentally measured EXAFS spectra.

A comparison of the RT and the near LNT Cu K-edge EXAFS spectra and the corresponding k-weighted Fourier transforms are shown in Fig. 5. Again, as anticipated, the amplitude of the EXAFS oscillations as well as the amplitude of the Fourier transforms increased when the specimen temperature decreased from RT to the LNT due to the quenching of the thermal motion of the atoms. These Fourier transforms display a major peak centered around 2.1 Å, which corresponds to the first coordination sphere of Cu–Ge interactions and a minor peak centered around 3.7 Å, which corresponds to more distant Cu–Ge interactions.

A comparison of the Fourier transforms of RT Cu and Ge EXAFS spectra and the LNT Cu and Ge EXAFS spectra are shown in Fig. 6. Clearly, the high degree of similarity between the Fourier transforms of Cu and Ge for each particular temperature is striking. As discussed earlier, both sets of Fourier transforms display a major and a minor peak corresponding to the first and second coordination spheres, respectively, confirming that Cu substitutes for framework Ge atoms. However, the position of the first peak in the Fourier transforms of Cu is shifted to a lower distance relative to that in the Fourier transforms of Ge. As will be confirmed from quantitative analysis of the spectra, the Cu–Ge distance is significantly shorter than the Ge–Ge distance.

The local structure parameters of Cu and Ge in $Cs_8Na_{16}Cu_5Ge_{131}$ are summarized in Table 2. In this table, we also included the local structure parameters of elemental Ge for comparison purposes. Comparisons of Fourier transforms of experimental spectra and simulation (fit data) are shown in Fig. 7.

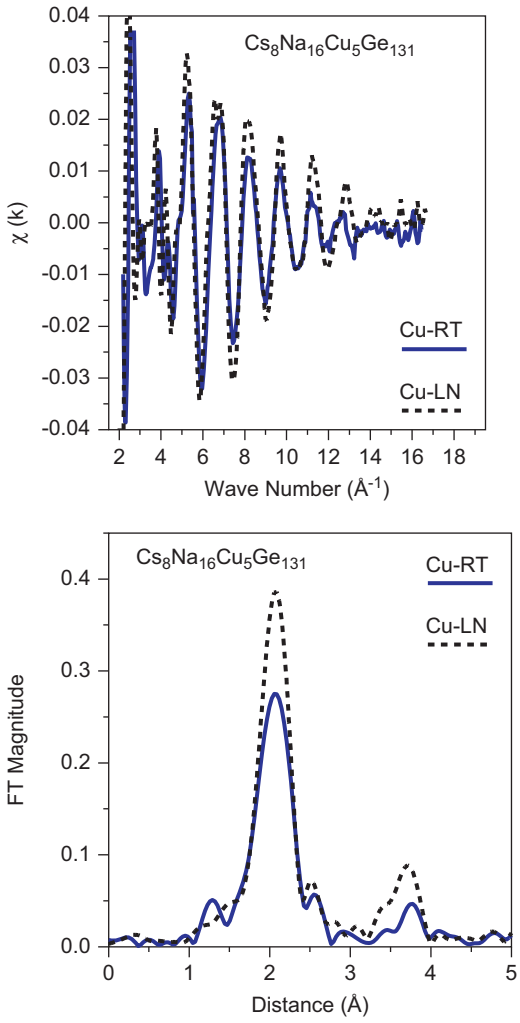

Fig. 5. Comparison of Cu K-edge EXAFS (top) and Fourier transforms (bottom) for $Cs_8Na_{16}Cu_5Ge_{131}$ collected at room temperature (RT) and near the temperature of liquid nitrogen (LN).

4. Discussion

Within the uncertainty in the data, the many body amplitude reduction factor, S_0^2, for Cu is similar to that of Ge in the clathrate specimen. This a clear indication that the amplitude of the Ge EXAFS signal is not reduced by thickness inhomogeneity as a result of the large Ge edge jump of 3.2 for our clathrate sample. The value of S_0^2 for elemental Ge is slightly outside the range obtained for Ge in the clathrate specimen but this could be due to the higher degree of correlation between S_0^2 and the disorder in the case of elemental Ge since, in this case, the XAFS measurements were made only at RT.

Our analysis for elemental Ge reveals a RT first shell Ge–Ge distance of 2.444 Å, which is in excellent agreement with the well-established crystalline value of 2.450 Å [29]. The RT first shell Ge–Ge distance of 2.486 Å for the clathrate is also in excellent agreement with the weighted average distance of the three Ge sites, which is calculated to be also 2.486 Å. The RT Cu–Ge

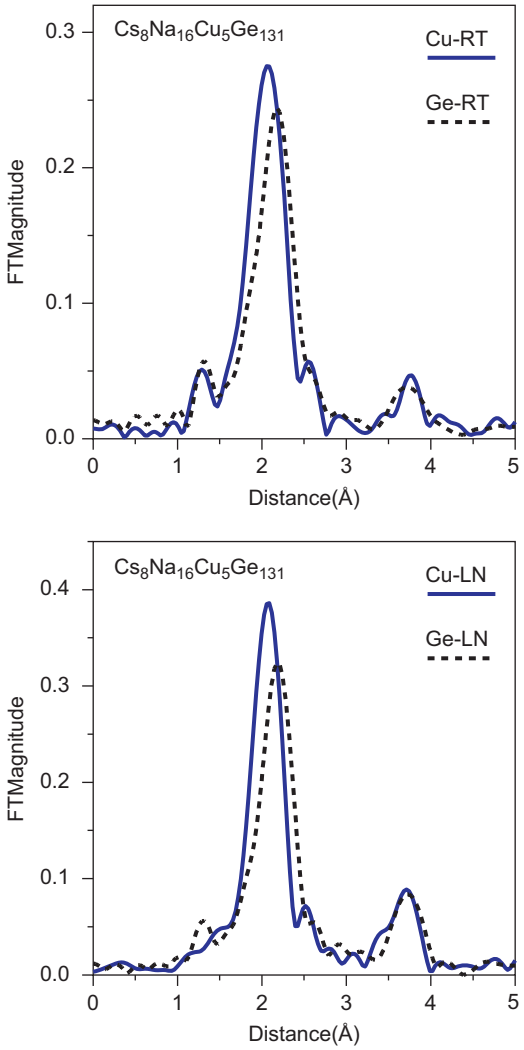

Fig. 6. Comparison of Fourier transforms of Cu *K*-edge and Ge *K*-edge EXAFS spectra for $Cs_8Na_{16}Cu_5Ge_{131}$ collected at room temperature (RT) and near the temperature of liquid nitrogen (LN).

distance of 2.354 Å, however, is significantly smaller than the RT Ge–Ge distance of 2.486 Å. The Cu–Ge distance is also significantly smaller than the well-established elemental Cu–Cu first shell distance of 2.556 Å [34]. The Cu–Ge distance is smaller by 0.132 Å from the Ge–Ge distance in $Cs_8Na_{16}Cu_5Ge_{131}$ and by 0.202 Å from the elemental Cu–Cu distance. This shorter Cu–Ge distance is consistent with the small reduction in the lattice parameter for $Cs_8Na_{16}Cu_5Ge_{131}$ ($a = 15.42000$ Å) relative to the parent compound $Cs_8Na_{16}Ge_{136}$ ($a = 15.49263$ Å) [11]. On the basis of these results, we conclude that a local distortion in the Ge framework of the clathrate is created in the proximity of the Cu atoms. In spite of such a local distortion, the RT as well as the LNT disorders for the Cu–Ge pair are essentially the same as those for the Ge–Ge pair within the uncertainty in our results. The total disorder consists of a temperature independent static term and a temperature dependent thermal term, which can be extracted separately by appropriately analyzing the temperature dependence of XAFS spectra. The microscopic Debye and Einstein temperatures for the Cu–Ge and Ge–Ge interactions are determined by modeling the temperature dependence of the thermal term using the Debye and Einstein models for lattice vibrations, respectively [35]. Accordingly, our results for the static disorder, thermal disorder, and total disorder for the Cu–Ge and Ge–Ge pairs are summarized in Table 3. The large uncertainties in the

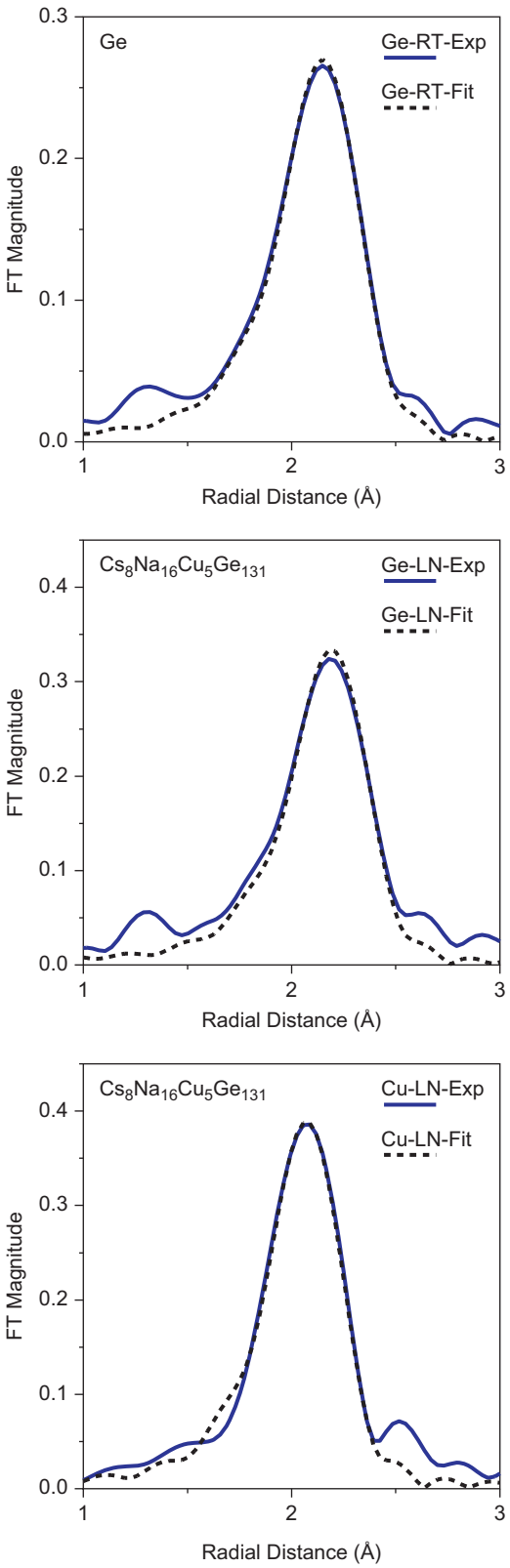

Fig. 7. Comparison of experimental and simulated Fourier transforms of Ge *K*-edge EXAFS spectra for Ge powder as well as those of the Ge *K*-edge and Cu *K*-edge EXAFS spectra for $Cs_8Na_{16}Cu_5Ge_{136}$. The simulated data were derived using the local structure parameters listed in Table 2.

Debye and Einstein temperatures are due to the limited number of temperature dependent EXAFS data sets (RT and LNT) we used in modeling the thermal disorder. The Debye temperatures for both

Table 3
Summary of the static disorder (σ^2_{static}), thermal disorder ($\sigma^2_{thermal}$), total disorder (σ^2_{total}), Debye temperature (θ_D), and Einstein temperature (θ_E) for the Cu–Ge and Ge–Ge pairs in $Cs_8Na_{16}Cu_5Ge_{131}$ type II clathrate

Lattice vibrations model	X–Y pair	σ^2_{static} (10^{-3} Å^2)	$\sigma^2_{thermal}$ (10^{-3} Å^2)	σ^2_{total} (10^{-3} Å^2)	θ_D or θ_E (K)
Debye model	Cu–Ge (RT)	0.36 ± 0.35	3.99	4.35	427 ± 32
	Cu–Ge (LN)		1.97	2.33	
Debye model	Ge–Ge (RT)	0.80 ± 0.47	3.74	4.54	428 ± 40
	Ge–Ge (LN)		1.84	2.65	
Einstein model	Cu–Ge (RT)	0.11 ± 0.35	4.23	4.34	333 ± 24
	Cu–Ge (LN)		2.21	2.32	
Einstein model	Ge–Ge (RT)	0.60 ± 0.47	3.94	4.54	334 ± 30
	Ge–Ge (LN)		2.06	2.65	

Cu and Ge are similar to those observed for Ge and Ga in $Eu_8Ga_{16}Ge_{30}$ and $Sr_8Ga_{16}Ge_{30}$ and are characteristic of a stiff lattice [36]. The similarities in the degree of static disorder, Debye temperature, and Einstein temperature for the Cu–Ge and Ge–Ge pairs indicate that the local bonding environment for Cu is very similar to that for Ge. This is consistent with the observation that the estimated lattice contribution to thermal conductivity is relatively unaffected by Cu substitution (along with the relatively low concentration of Cu) [11].

Since Ge in the clathrate resides in three non-equivalent sites, it is of interest to determine whether Cu substitution in the Ge framework is random or preferential. That is, whether Cu substitution has a preference to any of the three Ge sites, namely, 96g, 32*e*, and 8*a*. To address this issue, we have calculated the theoretical EXAFS spectra and Fourier transforms for each of the three Ge sites. In addition, we calculated the theoretical EXAFS spectra and Fourier transforms of the weighted average for the three Ge sites. These calculations were made using all of the local structure parameters (i.e., single scattering contributions), which are listed in Table 1 for each site. In addition, we repeated the simulation including a number of multiple scattering (MS) contributions for each of the Ge sites. For the Ge1 site, the first few MS contributions have effective path lengths of 4.479 (×8), 4.489 (×2), 4.521 (×4), 4.540 (×12), 4.552 (×4), 4.664 Å (×6) with the degeneracy for each path is given in parenthesis. For the Ge2 site, the first few MS contributions have effective path lengths of 4.479 (×12), 4.489 (×6), 4.514 (×6), 4.521 (×6), 4.552 (×6), 4.642 (×6) and 4.738 Å (×12). For the Ge3 site, the first few MS contributions have effective path lengths of 4.489 (×24), 4.514 (×12), and 4.642 Å (×24). The MS paths with different angular geometry but the same path length were listed as a single MS path with the appropriate degeneracy. The disorders for all of the MS paths were assumed to be 0.01 Å^2, which is the sum of the disorders for the two legs forming the MS path. As mentioned before, the backscattering amplitudes and phase shifts for each pair of Ge–Ge, Ge–Na, and Ge–Cs were calculated using the FEFF code. In these calculations, the many body amplitude reduction factor, S_0^2, was set to the experimentally determined Ge value of 0.80. The disorders were set to 0.005 Å^2 for the first shell of tetrahedrally coordinated Ge–Ge interactions, 0.010 Å^2 for the more distant second shell of Ge–Ge interactions, and 0.020 Å^2 for both the Ge–Na and Ge–Cs interactions. The disorders were primarily selected to bring qualitative resemblance with the Fourier transforms of the experimentally measured EXAFS spectra. The higher degree of disorder for the Ge–Na and Ge–Cs interactions relative to the Ge–Ge interactions is consistent with the rattling behavior of the Na and Cs guest atoms inside the framework polyhedral cages [24,25]. Such a high degree of disorder was observed for the rattling Eu and Sr atoms in $Eu_8Ga_{16}Ge_{30}$ and $Sr_8Ga_{16}Ge_{30}$, respectively [36].

Comparisons of the Fourier transforms of the theoretical EXAFS spectra simulated using single scattering contributions for each of the Ge sites with those simulated including the MS contributions are shown in Fig. 8. Clearly, the relative trends observed in the amplitudes of the first and second shells in the case of the single scattering simulation are similar to those observed in the case of the simulation, which also included the MS contributions. As can be seen from the Fourier transforms data, it is extremely difficult to distinguish between the three Ge sites on the basis of the first

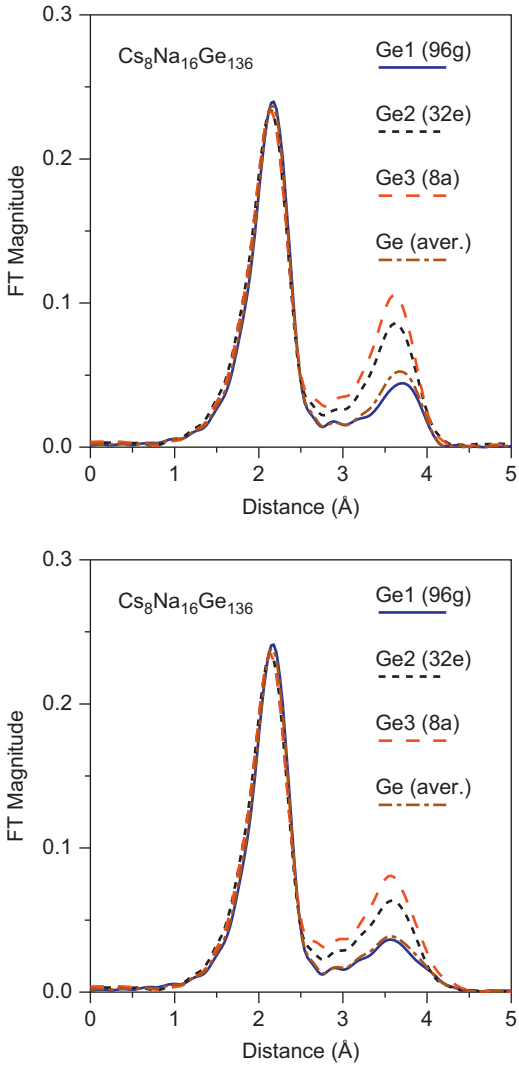

Fig. 8. Fourier transforms of EXAFS spectra simulated using only single scattering contributions (top) and those simulated using single scattering as well as MS contributions (bottom) of the Ge *K*-edge for $Cs_8Na_{16}Ge_{136}$. Simulated data for each individual site along with the weighted average of all contributions according to the site multiplicity are indicated.

peak in the Fourier transforms due the high degree of similarity in local structure parameters of the tetrahedral coordination of the three Ge sites. However, it could be possible to differentiate between the three Ge sites on the basis of the amplitude of the second peak in the Fourier transforms. The amplitude of this peak increased upon going from the Ge1 site, to the Ge2 site, and to the Ge3 site due to a gradual decrease in the degree of static disorder resulting from an increase in site symmetry for the three Ge sites in the same order (i.e., Ge1, Ge2, and Ge3, as indicated in Fig. 1 and Table 1). Due to the significantly higher multiplicity of the Ge1 site, the amplitude of the second peak in the Fourier transform for the weighted average of the three Ge sites is closer to that of the Ge1 site than that of the Ge2 or Ge3 site.

On the basis of the experimentally measured spectra (Fig. 6), the amplitude of the second peak in the Fourier transform for Cu is qualitatively quite similar to that of the second peak in the Fourier transform of Ge. This suggests that Cu is either (i) randomly substituting for Ge or (ii) preferentially substituting in the Ge1 site. In other words, preferential substitution of Cu in the Ge2 site or the Ge3 site can be excluded from consideration. These results are consistent with single crystal XRD studies that have shown preference for Ag and Ga substitution on the 96*g* (Ge1) site in type II germanium [9] and silicon [10] clathrates, respectively.

5. Conclusion

K-edge extended X-ray absorption fine structure spectra are reported for both Cu and Ge in the type II clathrate $Cs_8Na_{16}Cu_5Ge_{131}$. Analysis of the EXAFS data confirms that Cu is incorporated substitutionally on the Ge framework in this compound, with the estimated Cu concentration in good agreement with the expected Cu:Ge ratio of 5:131. The average first nearest neighbor distance for Cu appears approximately 0.13 Å shorter than that for Ge, indicating a local distortion around the Cu substituent. However, Cu–Ge and Ge–Ge disorder parameters remain similar. Preferential occupation of Cu at the 32*e* and 8*a* sites is excluded by comparison of experimental and simulated Fourier transformed data, consistent with previous single crystal results on framework substituted type II clathrates.

Acknowledgments

A.N.M acknowledges financial support by the Carderock Division of the Naval Surface Warfare Center's In-house Laboratory Independent Research Program administrated under ONR's Program Element 0601152N. M.B. and G.S.N. acknowledge support from the US Department of Energy under Grant no. DE-FG02-04ER46145. M.B. acknowledges support from the University of South Florida Presidential Doctoral Fellowship. The XAS experiments were conducted at the National Synchrotron Light Source of Brookhaven National Laboratory, which is supported by the US Department of Energy, Office of Basic Energy Sciences, under Contract no. DE-AC02-98CH10886.

References

[1] G.S. Nolas, J.L. Cohn, G.A. Slack, S.B. Schujman, Appl. Phys. Lett. 73 (1998) 178–180.
[2] J.L. Cohn, G.S. Nolas, V. Fessatidis, T.H. Metcalf, G.S. Slack, Phys. Rev. Lett. 82 (1999) 779–782.
[3] S. Paschen, W. Carrillo-Cabrera, A. Bentien, V.H. Tran, M. Baenitz, Y. Grin, F. Steglich, Phys. Rev. B 64 (2001) 214404-1–214404-11.
[4] S. Srinath, J. Gass, J. Rebar, G.T. Woods, H. Srikanth, G.S. Nolas, J. Appl. Phys. 99 (2006), 08K902-1–08K902-3.
[5] H. Kawaji, H.-O. Horie, S. Yamanaka, M. Ishikawa, Phys. Rev. Lett. 74 (1995) 1427–1429.
[6] G.S. Nolas, G.A. Slack, S.B. Schujman, in: T.M. Tritt (Ed.), Semiconductors and Semimetals, vol. 69, Academic Press, San Diego, 2000, p. 255.
[7] G.S. Nolas, in: M.G. Kanatzidis, S.D. Mahanti, T.P. Hogan (Eds.), Chemistry, Physics, and Materials Science of Thermoelectric Materials: Beyond Bismith Telluride, Kluwer Academic Publishers/ Plenum Publishers, New York, 2003, pp. 107–120.
[8] M. Beekman, G.S. Nolas, J. Mater. Chem. 18 (2008) 842–851.
[9] M. Beekman, W. Wong-Ng, J.A. Kaduk, A. Shapiro, G.S. Nolas, J. Solid State Chem. 180 (2007) 1076–1082.
[10] S. Bobev, J. Meyers Jr., V. Fritsch, Y. Yamasaki, in: Proceedings of the International Conference on Thermoelectrics, vol. 24, 2006, p. 48.
[11] M. Beekman, J.A. Kaduk, J. Gryko, W. Wong-Ng, A. Shapiro, G.S. Nolas, J. Alloys Comp. (2008), doi:10.1016/j.jallcom.2008.02.072, in press.
[12] K. Biswas, C.W. Myles, Phys. Rev. B 75 (2007) 245205-1–245205-7.
[13] D.E. Sayers, S.M. Heald, M.A. Pick, J.I. Budnick, E.A. Stern, J. Wong, Nucl. Instrum. Methods Phys. Res. 208 (1983) 631–635.
[14] M.E. Rose, M.M. Shapiro, Phys. Rev. 74 (1948) 1853–1864.
[15] E.A. Stern, K. Kim, Phys. Rev. B 23 (1981) 3781–3787.
[16] K.-Q. Lu, E.A. Stern, Nucl. Instrum. Methods 212 (1983) 475–478.
[17] J. Jaklevic, J.A. Kirby, M.P. Klein, A.S. Robertson, G.S. Brown, P. Eisenberger, Solid State Commun. 23 (1977) 679–682.
[18] M.O. Krause, J. Phys. Chem. Ref. Data 8 (1979) 307–327.
[19] Z. Tan, J. Budnick, S.M. Heald, Rev. Sci. Instrum. 60 (1989) 1021–1025.
[20] C.H. Booth, F. Bridges, Phys. Scr. T115 (2005) 202–204.
[21] J.A. Bearden, A.F. Burr, Rev. Mod. Phys. 39 (1967) 125–142.
[22] D.E. Sayers, B.A. Bunker. in: D.C. Koningsberger, R. Prins (Eds.), X-ray Absorption: Principles, Applications, Techniques of EXAFS, SEXAFS and XANES, Wiley, New York, 1988 (Chapter 6).
[23] J.W. Cook Jr., D.E. Sayers, J. Appl. Phys. 52 (1981) 5024–5031.
[24] T. Ressler, J. Synchrotron Radiat. 5 (2000) 118–122.
[25] T. Ressler, J. Phys. IV 7 (1997), C2-269–C2-270.
[26] E.A. Stern, M. Newville, B. Ravel, Y. Yacoby, D. Haskel, Physica B 208–209 (1995) 117–120.
[27] A.L. Ankudinov, B. Ravel, J.J. Rehr, S.D. Conradson, Phys. Rev. B 58 (1998) 7565–7576.
[28] A.L. Ankudinov, C.E. Boulden, J.J. Rehr, J. Sims, H. Hung, Phys. Rev. B 65 (2002) 104107-1–104107-11.
[29] P. Vilars, L.D. Calver, Pearson's Handbook of Crystallographic Data for Intermetallic Phases, vol. 3, American Society for Metals, Metals Park, OH, 1985, p. 2370.
[30] E.A. Stern, Phys. Rev. B 48 (1993) 9825–9827.
[31] W.H. McMaster, N. Kerr Del Grande, J.H. Mallett, J.H. Habbell, Compilation of X-ray Cross Sections, National Technical Information Services, US Department of Commerce, Springfield, VA, 1969.
[32] G.S. Nolas, D.G. Vanderveer, A.P. Wilkinson, J.L. Cohn, J. Appl. Phys. 91 (2002) 8970–8973.
[33] G.S. Nolas, C.A. Kendziora, J. Gryko, J.J. Dong, C.W. Myles, A. Poddar, O.F. Sankey, J. Appl. Phys. 92 (2002) 7225–7230.
[34] P. Vilars, L.D. Calver, Pearson's Handbook of Crystallographic Data for Intermetallic Phases, vol. 2, American Society for Metals, Metals Park, OH, 1985, p. 1023.
[35] E. Sevillano, H. Meuth, J.J. Rehr, Phys. Rev. B 20 (1979) 4908–4911.
[36] R. Baumbach, F. Bridges, L. Downward, D. Cao, P. Chesler, B. Sales, Phys. Rev. B 71 (2005) 024202-1–024202-19.